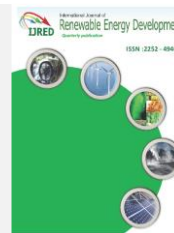




Contents list available at IJRED website






International Journal of Renewable Energy Development

Journal homepage: <https://ijred.undip.ac.id>



Research Article

Improving FTO/ZnO/In₂S₃/CuInS₂/Mo solar cell efficiency by optimizing thickness and carrier concentrations of ZnO, In₂S₃ and CuInS₂ thin films using Silvaco-Atlas Software

Maklewa Agoundedemba ^{a*} , Mazabalo Baneto ^{b,c} , Raphael Nyenge ^a , Nicholas Musila ^a , Kicoun Jean-Yves N'Zi Toure ^a 

^aDepartment of Physics, Kenyatta University P.O.Box 43844-00100 Nairobi, Kenya

^bDépartement de Physique, Laboratoire sur l'Energie Solaire, Université de Lomé, 01BP1515, Lomé-Togo

^cCentre d'Excellence Régional pour la Maîtrise de l'Electricité (CERME), Université de Lomé, 01BP1515, Lomé-Togo

Abstract. Optimization of optical and electrical properties of active semiconducting layers is required to enhance thin film solar cells' efficiency and consequently became the cornerstone for sustainable energy production. Computational studies are one of the ways forward to optimize solar cells' characteristics. In this study, Silvaco-Atlas, a powerful software that excels in both 2D and 3D electrical simulations of semiconductors has been used for the simulation in order to investigate the solar cell properties. The architecture of the solar cell simulated was FTO/ZnO/In₂S₃/CuInS₂/Mo. This study aims to optimize solar cell efficiency by optimizing film thicknesses and carrier concentrations via simulation. The designed solar cell was exposed to the presence of a sun spectrum of AM1.5 from a 1kW/m² incident power density at 300K. The thickness values of the window (ZnO), absorber (CuInS₂) and buffer (In₂S₃) layers were varied to record a solar cell's optimum thickness. The resulting FTO/ZnO/In₂S₃/CuInS₂/Mo solar cell formed by simulation is presented. The best efficiency and fill factor of the solar cell simulated were found to be 41.67% and 89.19%, respectively. The recorded values of current density and the open circuit voltage of the cell were 40.33mA/cm² and 1.15 V, respectively. Additionally, the maximum power of the simulated solar cell device was 41.68 mW. Optimization results revealed that the most efficient cell found was made up of a window layer with a thickness of 0.03μm, an absorber layer with a thickness of 6.0μm and a buffer layer with a thickness of 0.2μm. The optimized carrier concentration of ZnO, In₂S₃ and CuInS₂ was respectively 1e21 cm⁻³, 1e20 cm⁻³, 3e18 cm⁻³ and the optimized Al-doped ZnO value was 1e25 cm⁻³. The Absorption spectra indicated that the solar cell's peak absorption occurs between 350 nm and 1250 nm and presented a good external quantum efficiency (EQE) of around 84.52% to 92.83% which indicates good efficiency in the visible domain. This performance is attributed to the transparency of FTO, ZnO and good absorption of In₂S₃ and CuInS₂ thin films.

Keywords: Solar cell, efficiency, fill factor, open voltage, short circuit current density, Silvaco-Atlas.



@ The author(s). Published by CBIORE. This is an open access article under the CC BY-SA license (<http://creativecommons.org/licenses/by-sa/4.0/>).

Received: 29th August 2023; Revised: 30th Sept 2023; Accepted: 22nd Oct 2023; Available online: 29th Oct 2023

1. Introduction

Recently, absorber layers from chalcopyrite materials such as Cu(InGa)Se₂, CuInSe₂, and CuInS₂ used for solar cell elaboration have shown promising results because of their distinctive high absorbance, energy bandgap adequacy, defect chemistry and generating power at low cost with the least amount of raw resources used (Regmi *et al.*, 2020). Cu(In,Ga)Se₂ (CIGS) solar cells could achieve great efficiencies of more than 21.5% when exposed to AM1.5 sunlight (Amar *et al.*, 2021; Santhosh *et al.*, 2014).

Even though the accomplishment of CuInS₂ (CIS) solar cells at the moment is less effective than that of CIGS, they have gained interest on the basis of their affordability and suitability for replacing selenium (Se) with nonpoisonous sulfide (Song *et al.*, 2013). According to Chen *et al.*, (2014); Shang *et al.*, (2014) and Theresa *et al.*, (2005), CIS has a direct energy band gap in the range of 1.40-1.54 eV and its absorption coefficient is high, exceeding 10⁵ cm⁻¹ (Wijesundera and Siripala, 2004). Most of

these thin film thicknesses usually are much thinner than the conventional solar cells' thin films (mono-crystalline and poly-crystalline) which is ranged between 200 to 250 μm and are even in nanometers range values (L. Chen *et al.*, 2014; Hanket *et al.*, 2010). Depending on the application, the substrates employed for coating are FTO, ITO, metal, glass, or plastic.

CIS solar cells are highly efficient at converting sunlight into electricity, making them valuable for solar energy generation. They are constructed using thin-film technology, offering flexibility and lightweight design, allowing integration into various surfaces (Wijewardane & Kazmerski, 2023). Additionally, the use of abundant and cost-effective materials like indium and copper reduces manufacturing expenses. These solar cells can be configured in tandem or multi-junction setups, optimizing light absorption and energy conversion efficiency (Lv *et al.*, 2022). They also display excellent stability and durability in diverse environmental conditions, ensuring prolonged energy production (Lv *et al.*, 2022). Moreover, their lower toxicity

* Corresponding author
Email: amaklewa@gmail.com (A. Maklewa)

compared to other thin-film materials makes them more environmentally friendly, benefiting both production and disposal. Despite the different advantages listed above, researchers and manufacturers continue to explore ways to enhance the efficiency and cost-effectiveness of these thin-film solar cells. Hence, adding different materials are essential to boost its efficiency. In the last few years, solar cells were built with CIGS/CIS absorbers and CdS buffer layers which are advanced thin-film photovoltaic technology, with a conversion efficiency record of 20.10-22.60 % (Dambhare *et al.*, 2021; Jackson *et al.*, 2016; Tobbeche *et al.*, 2019). Dabbabi *et al.*, (2022) using CIS/CdS solar cell obtained better efficiencies of 29.62% experimentally and 38.6% by simulation using Silvaco- Atlas. The ternary chalcopyrite Cu(In, Ga)Se₂ (CIGS)-based thin-film technique has been discovered to have a proven yield of 20.8% coated on supple substrates and 22.3% on non-supple substrates (Dambhare *et al.*, 2021). With the use of the ADEPT 2.1 software, the buffer and absorber layer thicknesses were optimized. An efficiency of 23.67%-24.62% of CIGS solar were obtained with an absorber layer CIGS thickness of 1.6 μm and 0.04–0.06 μm of ZnO and ZnS respectively (Asaduzzaman *et al.*, 2017; Hosen *et al.*, 2017). Using Silvaco- Atlas software, 27.33% was obtained with an optimized values couple (thickness=0.025 μm , carrier concentration=6e17cm⁻³) and (thickness=4 μm , carrier concentration=1e18cm⁻³) for ZnS and CIGS respectively (Tobbeche *et al.*, 2019).

Many current researches led to the increase of cell's efficiency. For example, Sylla *et al.*, (2022) studied the CIGS solar cells with different thickness of CIGS layer using AFORS-HET software. An efficiency of 24.6% was obtained with thickness 3 μm . Nya *et al.*, (2019) simulated ZnS/CIGSe solar cell through the improvement of the ZnS and CIGS parameters like thickness utilizing SCAPS software and the conversion efficiency achieved was 26.3% with 5 nm thickness and 2.5 μm thickness respectively. More advancements are required for solar cells to operate more efficiently and to absorb more of the sunlight that strikes them (Dambhare *et al.*, 2021). In order to improve light transmission, many research groups were focused on successfully replacing the CdS layer with non-poisonous compounds with band gaps larger than CdS (Asaduzzaman *et al.*, 2017). According to numerous researchers, In₂S₃ thin film has been employed as a substitute to the CdS layer for CIS solar cells (Asaduzzaman *et al.*, 2017; Thomas *et al.*, 2015). In₂S₃ is used as an n-type layer and its thickness varies from 68nm to 470nm and energy band gap from 2.46eV to 2.73eV which is suitable for solar cell applications (Trigo *et al.*, 2008). Fluorine-doped tin oxide (FTO) and Zinc oxide (ZnO) thin films are promising candidates as transparent collectors of electrons and holes for CIS solar cells. They are more transparent and better conductors than tin oxide (SnO₂), titanium dioxide (TiO₂) (Dabbabi *et al.*, 2018). Therefore, to fabricate a solar cell with structure FTO/ZnO/In₂S₃/CIS/Mo, it needs to be simulated to have a precise idea of the parameters influencing the cell's efficiency in order to perform the experimental work.

Thus, optimizing parameters like thickness and doping concentration are required to achieve higher photon conversion efficiencies to make the solar cell more efficient. For example, Nya *et al.*, (2019) found that for a ZnS buffer layer thickness of 5 nm and 0.5 μm of CuIn_{0.7}Ga_{0.3}Se₂ the efficiency was 21.42% and the fill factor was 82.16%; however, for a ZnS buffer layer thickness of 5 nm and 2.5 μm of CuIn_{0.7}Ga_{0.3}Se₂ the efficiency was 26.30% and a fill factor 85.15%. The ZnO buffer layer has produced the greatest energy conversion efficiency (24.62%) out of all the cells with different buffer layers (Boukourt, 2018). ZnO is very interesting material and can have various applications such as photocatalysts, electronics (Sutanto, Durri,

et al., 2016; Sutanto, Wibowo, *et al.*, 2016). According to the simulation findings, utilizing ZnS and ZnO buffer layer in place of CdS results in high performances of cells (Asaduzzaman *et al.*, 2017). In fact, choosing Silvaco-Atlas can be explained by how it supports multi-dimensional simulations (2D and 3D), which are essential for accurately modelling the electrical behavior of solar cells. In contrast, some software like SCAPS provides simulation only in 1D and does not give accurate results. Researchers can test and optimize solar cell designs in a virtual environment before moving on to physical prototypes which helps to reduce experimental costs. For other softwares, the users don't understand anything about the functionality behind the software and only varies the parameter values. In other words, these software works like a black box which is different from the case of Silvaco-Atlas allowing users to implement their own code or script.

In this work, FTO/ZnO/In₂S₃/CIS/Mo heterostructure solar cell was simulated using Silvaco-Atlas software and the consideration of the proper parameters of compounds involved in the solar cell were taken from experimental data of other groups' work. The motivation of the cell design introduced in this study is based on findings from prior work made by Khoshsirat *et al.*, (2015), who explored the impact of varying band gap values in the absorber and buffer layers on the performance of CIGS thin-film solar cells, using the SCAPS software. The obtained results indicated that introducing a graded band gap structure in both the absorber and buffer layers led to improved efficiency and overall performance compared to a cell with a uniform band gap structure. The aim of this study is to enhance solar cell efficiency by optimizing thickness and carrier concentration of the active layers such as the window layer (ZnO), buffer layer (In₂S₃) and absorber layer CuIn₂ (CIS) via simulation. The optimal thickness and carrier concentration were recorded by varying their values of each layer up to a given value. The designed CIS solar cell was optimized and the results obtained were validated using published experimental data.

2. Theoretical Frame work

Solar cells work as a p-n or p-i-n photodiode junction. The working principle of those categories of cells is stated in three main steps: (i) absorption of photons from sunlight, (ii) conversion of photons energy into electrical current and (iii) collection of photocurrents generated. First, the device should absorb photons from sunlight. In order for photons to be absorbed, their energy should exceed the energy band gap of the semiconductor. The relationship of the energy of the incoming light and the energy gap is described by Tauc equation as shown in equation (1) (Baishya *et al.*, 2018; Sutanto *et al.*, 2015; Grigorovici and Vancu, 1966).

$$\alpha h\nu = (h\nu - E_g)^n \quad (1)$$

where α is absorption coefficient, E_g is the energy band gap, $h\nu$ is the energy of the incoming light, and n is the constant which depend on the type of transition. Moreover, as indicated in Tauc equation, there are two main parameters in the material's absorption: the absorption coefficient and the energy band gap of the material. The two parameters are responsible in the loss of power in a solar cell. The absorption of photon leads to the second step of converting photons into electrical current which occur by generating a pair of electrons-holes. Finally, once the charge carriers are created, by attaching metallic contacts of the n and p sides, the electrical current supplied by the solar panel is collected and a charge can be fed by collecting this electrical

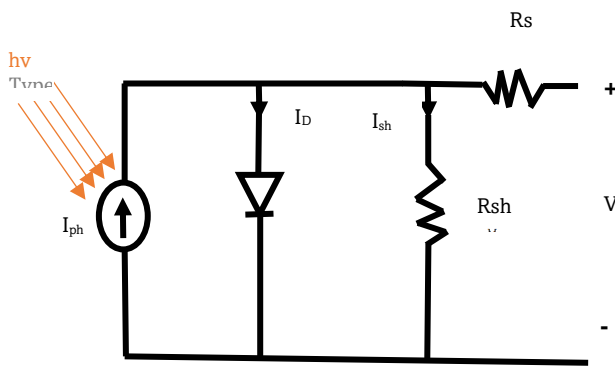


Fig. 1 One diode model of photovoltaic cell

current into the conductors towards it. Therefore, the other primary loss of power in a solar cell is caused by recombination of charge carriers which can be avoided with a proper design of the architecture of the cell.

The photocurrent is the current generated in the cell when it is illuminated. This cell is represented by Figure 1 which is a simple model of a solar cell called one diode model. Under the influence of incoming radiation, the current source (I_{ph}) symbolizes the creation of electrons-holes in the PV cell. These charge carriers recombine at a forward-bias voltage ($V+I.R_s$). The recombination of charge carriers is represented by the shunt diode. The shunt resistor (R_{sh}) indicates an elevated current channel across the semiconductor that flows through mechanical flaws, material dislocations, or crystal degradation in the border. The R_s stands for series resistance at the semiconductor's top surface, particularly in the junction between the semiconductor and metal (Boyd *et al.*, 2011; Stutenbaeumer and Mesfin, 1999; Tchakpedeou *et al.*, 2022).

R_s and R_{SH} of solar cell are responsible for loss process that affects the fill factor, efficiency and therefore the open-circuit voltage (V_{OC}) (Stutenbaeumer & Mesfin, 1999; Wang & Xuan, 2017) which on the other hand is related to the proper design of the solar cell structure. Then it's necessary to investigate the optimization of parameters of the solar cell, such as the thickness of compounds made up, their optical properties and the doping rate to enhance the current of the cell. Silvaco-atlas is one of the best software programs that allows simulating so as to determine the suitable device and optimized parameters. The results from that give an insight of the current produced by the device, avoiding preliminary experimentations and the accompanying costs. Silvaco-Atlas is a semiconductor simulation tool which solves in two and three dimensions three equations: Poisson, continuity, and transport equations at each node (Silvaco, 2019; Taraque *et al.*, 2019). The Poisson equation used is stated by equation (2).

$$\Delta V = -\frac{q}{\epsilon} (p - n + N_D^+ - N_A^-) \quad (2)$$

The continuity equations used in the simulation are shown in equation (3) and (4).

$$\frac{\delta n}{\delta t} = +\frac{1}{q} \left(\frac{\partial J_n}{\partial x} + \frac{\partial J_n}{\partial y} \right) + G_n - R_n \quad (3)$$

$$\frac{\delta p}{\delta t} = +\frac{1}{q} \left(\frac{\partial J_p}{\partial x} + \frac{\partial J_p}{\partial y} \right) + G_p - R_p \quad (4)$$

The transport equations are given by the conduction equations (drift equations) plus the diffusion equations which are stated in equations (5) and (6).

$$J_n = qn\mu_n E + qD_n \frac{\partial n}{\partial y} \quad (5)$$

$$J_p = qp\mu_p E + qD_p \frac{\partial p}{\partial y} \quad (6)$$

where $D_n = \frac{kT}{q} \mu_n$ and $D_p = \frac{kT}{q} \mu_p$ represent the diffusion coefficient of electrons and holes, respectively. The p and n are the electron and hole concentrations, N_D^+ is the ion donor concentration, and N_A^- is the ion acceptor concentration, J_n and J_p are current density of electrons and holes respectively. G is the generation rate, R is recombination rate, μ is charge mobility and E is the electric field.

The I-V characteristic of a cell can be obtained by Equation (7) (Belkassmi *et al.*, 2017; Boyd *et al.*, 2011; Dash & Ali, 2014).

$$I = I_{ph} - I_0 \left[e^{\frac{(V+IR_s)}{a}} - 1 \right] - \frac{(V+IR_s)}{R_{sh}} \quad (7)$$

where $a = \frac{nKT}{q}$ is the modified ideality factor, k is the Boltzmann constant, T is the cell temperature, q is the electron's charge and n is the diode ideality factor.

3. Methodology

3.1 Materials

Materials used in this study are as follow: two transparent conductive oxides namely zinc oxide which is a II-IV semiconductor with a large bandgap (3.2-3.37 eV) (Sutanto *et al.*, 2015, 2017; Sutanto, Durri, *et al.*, 2016) with a transmittance of more than 80% in the visible region (Wai, 2022) and Fluorine-doped Tin Oxide (FTO). Indium sulfide (In_2S_3), copper indium sulfide ($CuInS_2$) and molybdenum (Mo) were also used to perform the experiments. The In_2S_3 is a non-poisonous, n-type semiconductor material of group III-VI with energy band gap around 2.0-2.65 eV (Revathi *et al.*, 2009; Sharma *et al.*, 2017) and $CuInS_2$ a p-type semiconductor which has an energy band gap of 1.47 eV (Thirumalaisamy *et al.* 2019). Two softwares were used to plot graphs namely Origin 2021 and the tool TonyPlot implemented in Silvaco. The Silvaco software used in our modelling has the following characteristics: Silvaco 5.0.10.R Copyright © 1984 – 2023.

3.2 Simulation

The acronym SILVACO standing for Silicon Valley Corporation is a software that allows to design, model and simulate the performance of semiconductor devices, before manufacturing the test prototypes. The studies of most semiconductor devices, as in this present work, were based on the simultaneous resolution of the Poisson equation and the continuity equation mentioned earlier. The program calculated, at each moment, at every space point and using a finite element method, the concentration of electrons and holes, as well as the value of the electrostatic potential. The Poisson equation defines the relationship between the potential and the carrier density, as shown in equation 2. The time evolution of the carrier densities follows the continuity equations defined by equations 3 and 4. To perform the simulation under the Silvaco-Atlas environment, we defined the cell structure, the numerical

Table 1
Simulation's input parameters

Parameters	Materials			
	ZnO	CuInS ₂	In ₂ S ₃	FTO
Energy Bandgap (eV) at 300K	3.3	1.48	2.66	3.95
Thickness (μm)	0.06	2.4	0.2	0.1
Electron Mobility (cm ² /V s)	100	100	4x10 ²	10
Hole mobility (cm ² /V s)	25	25	25	25
Affinity(eV)	4.7	4.50	4.65	4.44
Permittivity (F m ⁻¹)	9	13.6	13.5	9
Density of state of a Conduction band, Nc (cm ⁻³)	2.2 10 ¹⁸	2.2 10 ¹⁸	2 10 ¹⁹	2.2 10 ¹⁸
Density of state of Valance band, Nv (cm ⁻³)	1.8 10 ¹⁹	1.8 10 ¹⁹	2 10 ¹⁷	1.8 10 ¹⁹

(Ghavami & Salehi, 2019; Salim, 2017; Shang et al., 2014; Silvaco, 2019; Sutanto et al., 2015; Yang et al., 2022)

method, the result extraction and the visualization of figures. For the structure definition, various processes were established successively, which involved specifying the physical domain of the simulation, the different materials that make up the structure, the electrodes and the doping of different regions to create an appropriate mesh for studying the structure. To assure the accuracy of the outcomes, the meshing procedure was carried out with great care. To obtain reliable and accurate results, the mesh density was defined based on the variations of the physical quantities. However, the choice of meshing was made to strike a balance between execution speed and result accuracy. Once the meshing was done by creating vertical and horizontal line, each zone of the mesh was assigned to the different types of materials that make up the cell mentioned earlier. After specifying the regions and materials, at least one electrode was defined in contact with a semiconductor material. In this work, two electrodes, the anode and the cathode, were used. Indeed, the finite element method was used to solve the physical equations. Its basic principle is the discretization of the equations. Finally, results extraction was achieved using the "EXTRACT" command, and the figures were visualized using "TonyPlot".

In this section, some of the explanation of the physical models that have been used in the simulation are presented. The values of the input parameters used in this work are listed in Table 1. This simulation predicted the electrical behavior of FTO/ZnO/In₂S₃/CuInS₂/Mo cell by solving the Poisson, continuity and conduction equations. The defined overview of the FTO/ZnO/In₂S₃/CuInS₂/Mo heterojunction solar cell made is shown in Figure 2. The cell was formed by a p-i-n structure such as absorber layer CIS (p-type), window layer ZnO (n-type), buffer layer In₂S₃ (n-type), front contact FTO and back contact Mo. To enhance accuracy and confidence in the results, the optical input files including the extinction coefficient $k(\lambda)$ and the wavelength-dependent refractive index $n(\lambda)$ of ZnO, FTO, In₂S₃ and CIS materials used were from published works. The wavelength applied was in the range 200 nm to 1800 nm.

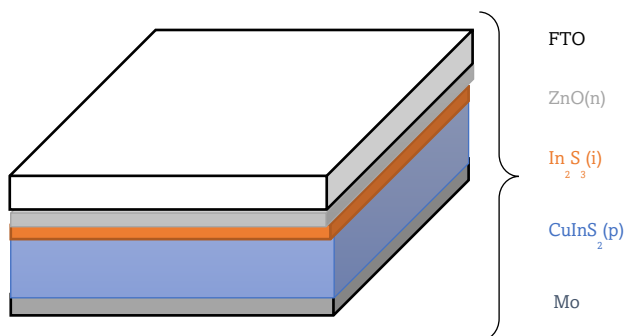


Fig. 2 Overview of the solar cell

The developed solar cell was lit to the presence of AM 1.5 sun spectrums of 1000 W/m² incident power density.

The efficiency of the cell and the fill factor were calculated using equations (8) and (9).

$$\eta = \frac{I_{mp} \times V_{mp} \times 10^8 W/cm^2}{1000W/m^2} \tag{8}$$

$$FF = \frac{I_{mp} \times V_{mp}}{V_{oc} \times I_{sc}} \tag{9}$$

where I_{mp} , V_{mp} are respectively the current and voltage at the maximum power point. I_{sc} and V_{oc} are respectively the short circuit current and open voltage of the cell. The maximum power was calculated using equation (10).

$$P_m = I_{mp} \times V_{mp} \tag{10}$$

The structure of the solar cell simulated in two dimensions using Silvaco-Atlas is shown in Figure 3. Each color of the structure in Figure 3 is for different compounds which make up the cell. After defining the structure, the meshes were defined into the cell. The result of a mesh created in the cell is shown in Figure 4. Therefore, the mesh created in Figure 4 made it possible to have many nodes in the form of matrix points which helped to solve equations 1 to 5. With a look at Figure 4 each vertical line and horizontal line are crossing at some points called nodes and all nodes form a mesh and which easily helped to solve the equations mentioned above. Meshes play an important role in obtaining accurate simulations. More meshes resulting more node and in consequence it gives more accurate results.

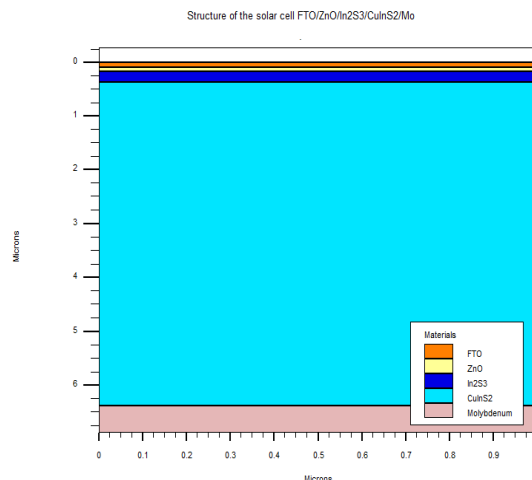


Fig.3 Structure of the solar cell FTO/ZnO/In₂S₃/CIS/Mo

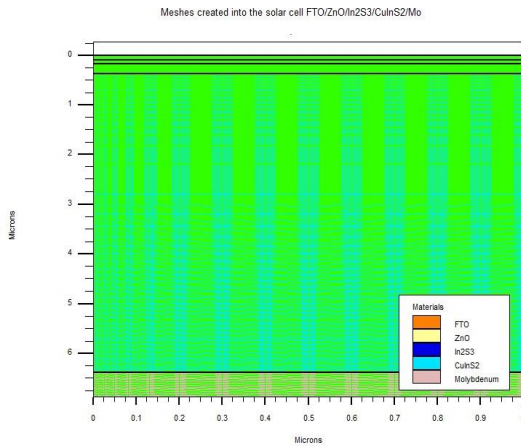


Fig.4 Mesh created into the cell

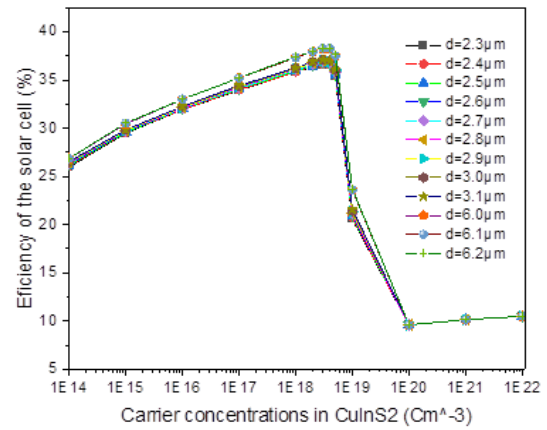


Fig. 6 Efficiency of the cell against the carrier concentration of CIS with different thicknesses.

4. Results and Discussion

4.1 Absorption region of the solar cell

As shown in Figure 5, the maximum peak of absorption of the optical wavelength occurred between 350 nm and 1250 nm, which correspond to the visible region (380 nm-800 nm) and the shortest wavelength in the infrared region. Some small absorption peaks occurred in ultraviolet region between 200 nm and 350 nm. The collection of photons with small wavelengths can be due to the fact that ZnO layer has wide band gap which was able to absorb photons with small wavelengths to generate electrons from the band of valence to the conduction band. The absorption of photons of wavelengths between 350-1250nm was due to the transparency of FTO, ZnO and the small band gap of In₂S₃ and CuInS₂. From the results above and the analysis of Figure 5, the main absorption region of FTO/ZnO/In₂S₃/CIS/Mo was between 350 nm and 1250 nm.

4.2 Optimum thickness of absorber layer CuInS₂

The thicknesses and charge carrier concentrations of FTO, ZnO, In₂S₃ and Molybdenum (Mo) were fixed at 0.1 μm, 0.05 μm, 0.2 μm, 0.5 μm and 5e22 cm⁻³, 5e17 cm⁻³, 9e18 cm⁻³, respectively based on the result obtained by Dabbabi *et al.*, (2017, 2022). Both thickness and carrier concentration variation of CuInS₂ were done on a scale of 0.1μm and log₁₀ cm⁻³ respectively, as shown in Figure 6. Indeed, Figure 6 depicts the

fit of the solar cell’s efficiency versus a carrier concentration of the absorber layer at different thicknesses. Additionally, looking at Figure 6, the observation was that as the carrier concentration of the absorber layer CIS increases, the efficiency of the cell also gradually increases up to a maximum carrier concentration of 3e18 cm⁻³ and beyond this value the efficiency decreases. At the same time, as the thickness increases the efficiency of the cell increases gradually up to 38.28% with a thickness 6.0 μm and remain constant up to the thickness 6.2 μm. This can be explained by the fact that the larger is the absorber layer thickness, the greater is the number of absorbed photons which leads to the generation of a higher number of charge carriers contributing to the enhancement of the efficiency. Since the maximum efficiency was for 6.0 μm thickness and 3e18 cm⁻³ carrier concentration of CIS, hence, these two values were retained as optimum thickness and concentration of CuInS₂ in an FTO/ZnO/In₂S₃/CIS/Mo solar cell. This result is in good agreement with the values obtained by (Dabbabi *et al.*, 2017, 2022; Onuma *et al.*, 2001; Shang *et al.*, 2014) range from 2μm to 9μm.

4.3 Optimization of In₂S₃ layer

Knowing the perfect CuInS₂ thickness of this solar cell in the first step, then the second step procedure used followed the same way as the previous one. The thickness and carrier concentration of CuInS₂ was fixed at 6.0 μm and 3e18 cm⁻³. The

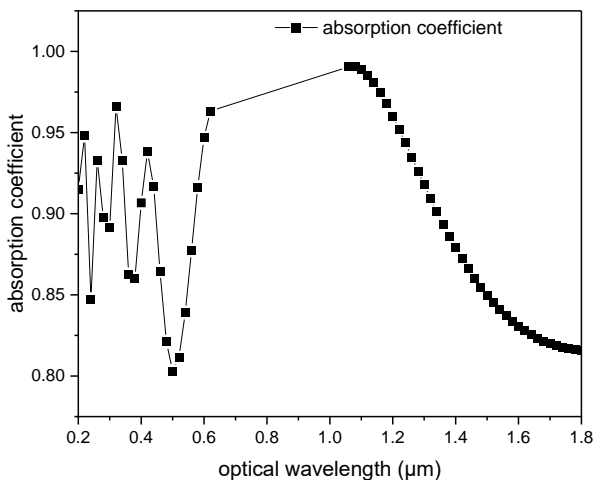


Fig. 5 Optical wavelength against absorption of the solar cell

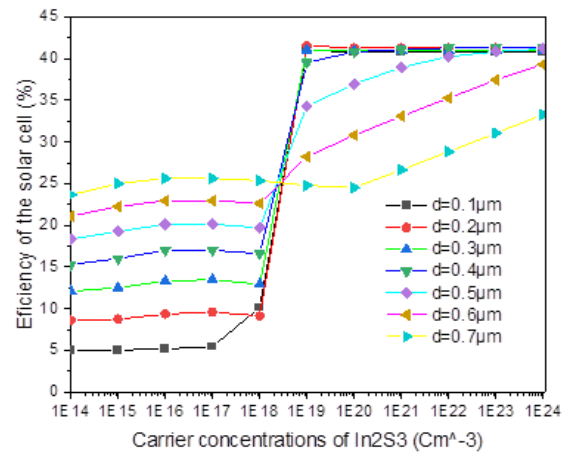


Fig.7 Efficiency of the cell vs the carrier concentration of In₂S₃ with different thicknesses.

thickness and carrier concentration of FTO, ZnO, In_2S_3 , Mo remained the same as previously based on the results obtained by Dabbabi *et al.*, (2017, 2022). Here, the variations of the In_2S_3 layer's thickness and the concentration were done on a scale of $0.1\mu\text{m}$ and $\log_{10}\text{ cm}^{-3}$, respectively. Indeed, looking at Figure 7, the observation made was that, as the carrier concentration of the In_2S_3 layer increases, the efficiency of the cell also increases to a maximum of 41.28% with carrier concentration of $1\text{e}20\text{ cm}^{-3}$, and then beyond this maximum value the efficiency remained constant. Moreover, for low carrier concentrations as the thickness increases the efficiency increases too. In contrast from $1\text{e}20\text{ cm}^{-3}$ carrier concentrations, the solar cell's efficiency increases for In_2S_3 thickness between $0.1\mu\text{m}$ to $0.2\mu\text{m}$ and then the efficiency decreases for In_2S_3 thickness beyond $0.2\mu\text{m}$. This can be due to the fact that as the In_2S_3 thickness increases the probability of the charge carrier recombination is high. It can be concluded that $0.2\mu\text{m}$ thickness and $1\text{e}20\text{ cm}^{-3}$ are the optimize values which is in agreement with values obtained by (Dabbabi *et al.*, 2021; Revathi *et al.*, 2010) who obtained $0.2\text{-}0.5\mu\text{m}$ thickness and $9\text{e}18\text{ cm}^{-3}$ carrier concentration.

4.4 Optimization of the ZnO layer

Finally, in the third step the couple (thickness, carrier concentration) of CuInS_2 and In_2S_3 were ($6.0\mu\text{m}$, $3\text{e}18\text{ cm}^{-3}$) and ($0.2\mu\text{m}$, $1\text{e}20\text{ cm}^{-3}$) respectively. The thickness and carrier concentration of FTO and Mo remained the same as previously based on the results obtained by Dabbabi *et al.*, (2017, 2022). Here, the variations of the ZnO layer's thickness and the concentration were done on a scale of $0.01\mu\text{m}$ and $\log_{10}\text{ cm}^{-3}$ respectively. Figure 8, shows that as the carrier concentration of the ZnO layer increases, the efficiency of the cell also increases to a maximum of 41.52% with $1\text{e}21\text{ cm}^{-3}$ carrier concentration. Beyond this value, the efficiency stills relatively constant. We remarked that, independently of the thickness, the different curves have the same behavior. For this step, the highest efficiency was obtained for $0.03\mu\text{m}$ thickness of ZnO with $1\text{e}21\text{ cm}^{-3}$ carrier concentration. This result is similar to that (Bouarissa and Daoudi, 2018; Dabbabi *et al.*, 2017, 2021) who obtained $0.01\text{-}0.1\mu\text{m}$ thicknesses and $5\text{e}17\text{ cm}^{-3}$ carrier concentration of ZnO.

4.5 Optimization of n-doped ZnO layer

In this section, the effect ZnO-doped thin films was investigated. The dopant used was aluminum and the concentration of the n dopant was varied from $1\text{e}14\text{ cm}^{-3}$ to $1\text{e}28\text{ cm}^{-3}$ with a scale of

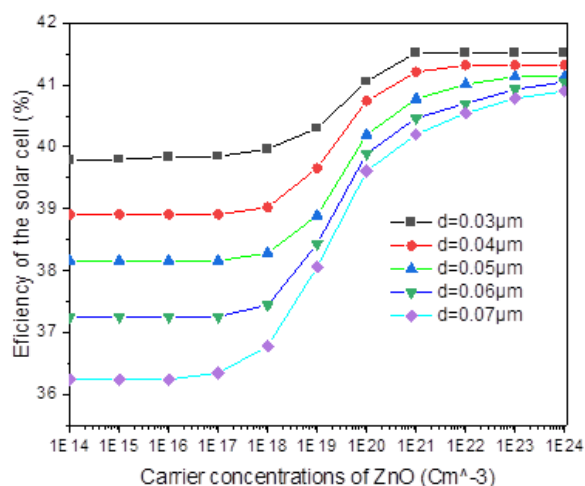


Fig. 8 Efficiency of the cell vs the carrier concentration of ZnO at different thickness

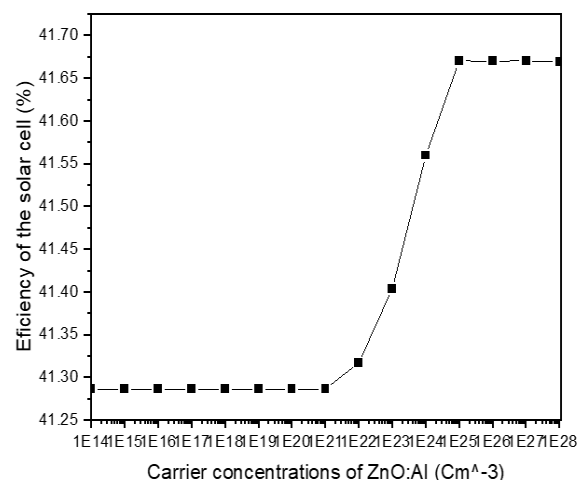


Fig. 9 Efficiency of the cell vs the carrier concentration of Al-doped ZnO

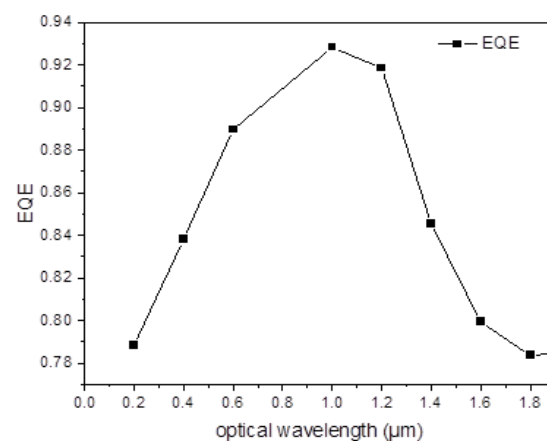


Fig.10 External Quantum Efficiencies of the cell

$\log_{10}\text{ cm}^{-3}$. Figure 9 shows the effect of the doping level on a solar cell's efficiency. As shown in Figure 9, the efficiency was constant up to $1\text{e}21\text{ cm}^{-3}$ dopant concentration. From $1\text{e}21\text{ cm}^{-3}$ to $1\text{e}25\text{ cm}^{-3}$ the efficiency increased drastically up to 41.67% and remained constant up to $1\text{e}28\text{ cm}^{-3}$. Considering this result, $1\text{e}25\text{ cm}^{-3}$ was retained as an optimum Al-doping concentration rate of ZnO in an FTO/ZnO/ In_2S_3 /CIS/Mo solar cell.

4.6 External Quantum Efficiency of the cell

The evaluation of the spectral response of the solar cell was done by plotting its External Quantum Efficiency (EQE) curve as shown in Figure 10. It can be observed that EQE increases in the wavelength range from $0.2\mu\text{m}$ to $1.0\mu\text{m}$ and then decreases. This can be due to the fact that the photons absorption was high in this domain as shown in Figure 5. A good spectral response varying from 79.00% to 92.83% was obtained in this domain, indicating good efficiency of the cell in the visible domain.

4.7 I-V curve of optimized FTO/ZnO/ In_2S_3 /CIS/Mo solar cell

The I-V characteristic of the solar cell is shown in Figure 11. The analysis of the curve presents a non-linear behaviour. Indeed, It can be observed three zones: zone1, zone2 and zone3 as indicated on the Figure 11. The first zone is the linear part of the curve which means that the cell behaved like a current generator. In other words, the current was nearly constant,

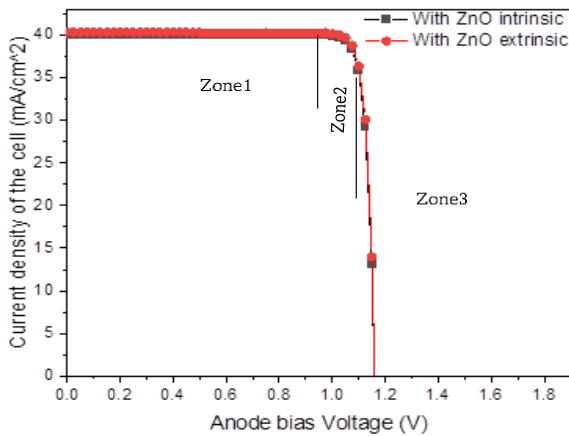


Fig. 11 I-V curve of FTO/ZnO/In₂S₃/CuInS₂/Mo solar cell

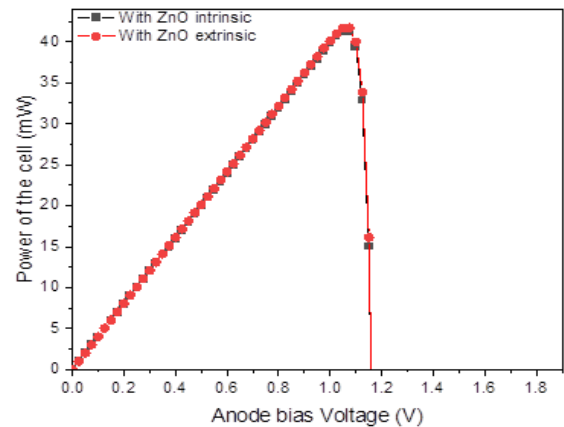


Fig. 12 Fitting of Power of solar cell FTO/ZnO/In₂S₃/CuInS₂/Mo vs Voltage

close to short-circuit current density (J_{sc}). The operation of the cell in that region resulted in low power, high currents and low voltages. The second zone is the exponential part of the curve which can be explained that in this region the solar cell behaved like a voltage generator in open circuit. The operation of the cell in this region resulted in low power, small currents and high voltages. Finally, in the last part of the curve zone 3, the operation of the cell resulted in high power, acceptable currents and voltages.

It appears that at zero current, the voltage was at its maximum value. This is known as the open-circuit voltage (V_{oc}) which represents the maximum voltage that the solar cell can generate when not connected to any load. We also observed that at zero voltage, the current was at its maximum value. This is known as the short-circuit current. Furthermore, it represents the maximum current that the solar cell can deliver when the terminals are directly connected together without any load. J_{sc} was mainly depending on the amount of light falling on the solar cell.

From this simulation as shown in Figure 11, the short circuit current density and the open circuit voltage (J_{sc} , V_{oc}) were approximately (40.00mA/cm², 1.15V) using ZnO intrinsic (black curve) and (40.33mA/cm², 1.15V) using ZnO extrinsic (red curve), respectively. The values of the efficiency of the solar cell with ZnO intrinsic and n-doped ZnO was found to be 41.28% and 41.67 %, respectively. Additionally, the fill factor which represents the overall performance of the solar cell, was found in this work to be 89.08% using ZnO intrinsic and 89.15% using ZnO extrinsic. So, it can be seen that the Al-doped ZnO has increased the efficiency, J_{sc} and FF of the solar cell.

4.8 Power of FTO/ ZnO/In₂S₃/CuInS₂/Mo cell

The power of the cell was calculated using the data generated in the simulation. Figure 12 depicts the fitting of the power against the bias voltage. We observe the maximum power point (MPP) on the power-voltage curve which represents the optimal operating point of the solar cell where it delivers the maximum power output. This point corresponds to a specific voltage (V_{mpp}) and current (I_{mpp}). The product of V_{mpp} and I_{mpp} gives the maximum power output of the solar cell. In this simulation, the couple (V_{mpp} , I_{mpp}) was found equal to (1.05V, 39.335 mA) using ZnO intrinsic (black curve) and (1.07499V, 38.7777mA) for ZnO extrinsic (red curve). The value of the maximum power output was found to be 40.3017 mW using ZnO intrinsic (black curve) and 41.6856mW for ZnO extrinsic (red curve).

It can be concluded that doping ZnO thin films increases the power of the solar cell.

4.9 Comparative study

The Figure 13 shows respectively, the I-V curve of the current work using ZnO intrinsic (black curve), ZnO extrinsic (green curve) and the simulation work from Dabbabi *et al.*, (2022) (red curve). It can be observed that the current and voltage are non-linear. Examining this developed solar cell, the current efficiency obtained with ZnO intrinsic and ZnO extrinsic were respectively 41.67% and 41.28%. These efficiencies are the key parameters that indicate how effectively the cell converts sunlight into electrical energy. The solar cell efficiency obtained in the current work is superior to the efficiency of some previous work. For example, Dabbabi *et al.*, (2022) got from experiment 29.62% as efficiency and from simulation 38.20%. Furthermore, Ghavami and Salehi, (2019) from simulation got 31.78% and Di Iorio *et al.*, (2017) from experiment got 2.8%. Moreover, the pair of values (J_{sc} , V_{oc}) obtained for ZnO intrinsic and extrinsic which are respectively (40.00mA/cm², 1.15V); (40.33mA/cm², 1.15V) are shown in Figure 13. These values are greater than those obtained recently by researchers such as Dabbabi *et al.*, (2022) who obtained (41.15 mA/cm², 1.00767 V) experimentally and (36.80 mA/cm², 1.01202V) from simulation. Moreover,

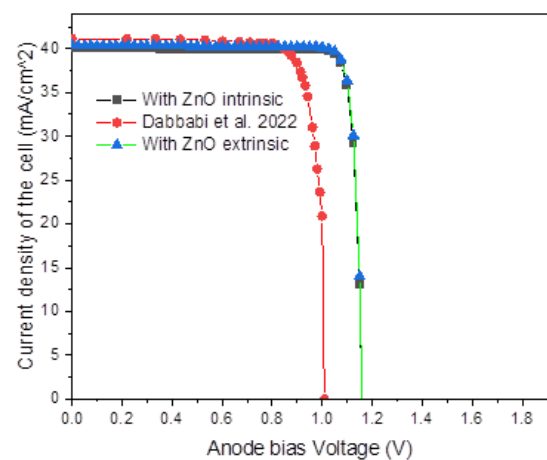


Fig. 13 Comparison of the I_V curve of solar cell FTO/ZnO/In₂S₃/CuInS₂/Mo and Dabbabi *et al.* 2022

Ghavami and Salehi, (2019) also found from simulation (39.89910 mA/cm², 0.91901 V). The fill factor was found in this work as 89.08% using ZnO intrinsic and 89.15% using ZnO extrinsic, whereas Dabbabi *et al.*, (2022) found with CIS solar cell 66.84% from experiment and 84.18% from simulation. A spectral response was obtained varying from 79.00% to 92.83% which is in good agreement with Dabbabi *et al.*, (2022) who obtained the spectral response of CIS solar cell from 85% to 90%. Phung and Do, (2021) study SCAPS simulation of ZnO / In₂S₃ / Cu₂Sn₃S₇ / Mo solar cell and found with 0.2 μm ZnO thickness, 0.1 μm In₂S₃ thickness the conversion efficiency η_{max} = 18.0 % with Voc = 0.98 V, Jsc = 31.2 mA/cm² and FF = 58.8 %. We can see that all the metric parameters found is less than values obtained in this study using Silvaco-Atlas.

5. Conclusion

The aim of this work was to perform numerical simulation and optimization of the main parameters of solar cells such as thickness, carrier concentration, the efficiency, fill factor, open circuit voltage and short circuit current. The FTO/ZnO/In₂S₃/CuInS₂/Mo solar cell simulation using Silvaco-Atlas software is presented. The created model can forecast how well solar cells would work at various thicknesses and carrier concentrations. Then, the optimal parameters of various layers of concern were determined and presented. It was found that the new design solar cell performed better with the optimum thicknesses of window layer, an absorber layer and a buffer layer of 0.03 μm, 6.0 μm and 0.2 μm, respectively. The efficiency, the fill factor, the current density and the open circuit voltage of the simulated solar cell was slightly greater compared to other's work. Al-doped ZnO increases efficiency of the cell. In addition, compounds' thickness and carrier concentration in CIS solar cell influence its efficiency. It was found that the thickness and carrier concentration of layers in the cell constructed FTO/ZnO/In₂S₃/CuInS₂/Mo has a crucial part in deciding how well it performs. From these results of the simulation it is recommended that to enhance solar cell efficiency, Isc, Voc and FF, some main parameters of its material should be optimized. However, an extensive study of electron lifetime in this solar cell and doping ZnO with some new material that can allows to capture most of the wavelengths in the ultraviolet region will improve this work. These results can be compared and can be validated by carrying out the experimental works.

Acknowledgments

The authors acknowledge the Partnership for Applied Sciences, Engineering, and Technology (PASET) and Regional Scholarship and Innovation Fund (RSIF) for the financial support.

Author Contributions: Maklewa Agoundedemba.: Conceptualization, methodology, formal analysis, writing—original draft, Mazabalo Baneto; review—editing and validation, Raphael Nyenge; supervision review—editing and validation, Nicholas Musila; supervision review—editing and validation, Toure Kicoun Jean-Yves N'Zi; review-editing. All authors have read and agreed to the published version of the manuscript.

Funding: The Partnership for Applied Sciences, Engineering, and Technology (PASET) and Regional Scholarship and Innovation Fund (RSIF) provided funding for this study.

Conflicts of Interest: The authors declare no conflict of interest. The funders had no role in the design of the study; in the collection, analyses,

or interpretation of the data; in the writing of the manuscript; and in the decision to publish the results.

References

- Amar, H., Amir, M., Ghodbane, H., Babes, B., Kateb, M. N., Zidane, M. A., & Rauane, A. (2021). Electrical characteristics study of heterojunction solar cells CdS/CIGS. *Semiconductor Physics, Quantum Electronics and Optoelectronics*, 24(04), 457–465. <https://doi.org/10.15407/spqeo24.04.457>
- Asaduzzaman, M., Hosen, B., Ali, K., & Bahar, A. N. (2017). Non-Toxic Buffer Layers in Flexible Cu (In , Ga) Se 2 Photovoltaic Cell Applications with Optimized Absorber Thickness. *International Journal of Photoenergy*, 2017(4561208), 1–8. <https://doi.org/10.1155/2017/4561208>
- Baishya, K., Ray, J. S., Dutta, P., Das, P. P., & Das, S. K. (2018). Graphene-mediated band gap engineering of - WO 3 nanoparticle and a relook at Tauc equation for band gap evaluation. *Applied Physics A*, 0(0), 0. <https://doi.org/10.1007/s00339-018-2097-0>
- Belkassmi, Y., Gueraoui, K., Elmaimouni, L., & Hassanain, N. (2017). Modeling and Simulation of Photovoltaic Module Based on One Diode Model Using Matlab / Simulink. *International Conference on Engineering & MIS (ICEMIS)*, Monastir(Tunisia 2017), 1–6. <https://doi.org/10.1109/ICEMIS.2017.8272965>
- Bouarissa, A. G. N., & Daoudi, A. N. F. (2018). Characteristics and optimization of ZnO / CdS / CZTS photovoltaic solar cell. *Applied Physics A*, 0(0), 0. <https://doi.org/10.1007/s00339-018-1626-1>
- Boukourt, N. (2018). Electrical Characterization of n-ZnO / c-Si 2D Heterojunction Solar Cell by Using TCAD Tools. *Silicon*, 2018(September), 1–7. <https://doi.org/10.1007/s12633-017-9750-7>
- Boyd, M. T., Klein, S. A., Reindl, D. T., & Dougherty, B. P. (2011). Evaluation and validation of equivalent circuit photovoltaic solar cell performance models. *Journal of Solar Energy Engineering, Transactions of the ASME*, 133(2). <https://doi.org/10.1115/1.4003584>
- Chen, H., Wang, C., Wang, J., Hu, X., Zhou, S., Chen, H., Wang, C., Wang, J., Hu, X., & Zhou, S. (2014). First-principles study of point defects in solar cell semiconductor CuInS₂ First-principles study of point defects in solar cell semiconductor CuInS₂. *Journal of Applied Physics*, 084513(2012), 1–6. <https://doi.org/10.1063/1.4762001>
- Chen, L., Lee, J., Shafarman, W. N., Ag, A., In, C., Se, G., In, C., & Se, G. (2014). The Comparison of (Ag , Cu) (In , Ga) Se 2 and Cu (In , Ga) Se 2 Thin Films Deposited by Three-Stage Coevaporation. *IEEE Journal of Photovoltaics*, 4(1), 447–451. <https://doi.org/10.1109/JPHOTOV.2013.2280471>
- Dabbabi, S., Nasr, T. Ben, Ammar, S., & Kamoun, N. (2018). Synthesis and Characterization of Zinc-Tin-mixed oxides thin films. *Superlattices and Microstructures*. <https://doi.org/10.1016/j.spmi.2018.05.058>
- Dabbabi, S., Nasr, T. Ben, & Kamoun-Turki, N. (2017). Parameters optimization of CIGS solar cell using 2D physical modeling. *Results in Physics*, 7(July), 4020–4024. <https://doi.org/10.1016/j.rinp.2017.06.057>
- Dabbabi, S., Seboui, Z., Tlili, M., & Jebbari, N. (2021). A new optimization approach for high efficiency of FTO / InS / CIS heterojunction solar cells. *International Journal of Modelling and Simulation*, 00(00), 1–9. <https://doi.org/10.1080/02286203.2021.1945896>
- Dabbabi, S., Seboui, Z., Tlili, M., Jebbari, N., Garcia-Loureiro, A., & Kamoun, N. (2022). A new optimization approach for high efficiency of FTO/InS/CIS heterojunction solar cells. *International Journal of Modelling and Simulation*, 42(4), 561–569. <https://doi.org/10.1080/02286203.2021.1945896>
- Dambhare, M., Butey, B., & Moharil, S. V. (2021). Solar photovoltaic technology: A review of different types of solar cells and its future trends Solar photovoltaic technology: A review of different types of solar cells and its future trends. *Journal of Physics: Conference Series*, 1913(2021), 0–16. <https://doi.org/10.1088/1742-6596/1913/1/012053>
- Dash, R., & Ali, S. M. (2014). Comparative study of one and two diode

- model. *International Journal of Research in Engineering and Technology*, 03(10), 190–194. <http://www.ijret.org>
- Di Iorio, Y., Berruet, M., Gau, D. L., Spera, E. L., Pereyra, C. J., Marotti, R. E., & Vázquez, M. (2017). Efficiency Improvements in Solution-Based CuInS₂ Solar Cells Incorporating a Cl-Doped ZnO Nanopillars Array. *Physica Status Solidi (A) Applications and Materials Science*, 214(12). <https://doi.org/10.1002/PSSA.201700191>
- Ghavami, F., & Salehi, A. (2019). High-efficiency CIGS solar cell by optimization of doping concentration, thickness and energy band gap. *Modern Physics Letters B*, 2050053(December), 1–11. <https://doi.org/10.1142/S0217984920500530>
- Grigorovici, R., & Vancu, A. (1966). Optical Properties and Electronic Structure of Amorphous Germanium. *Phys. Stat. Sol.*, 15(627), 627–637. <https://doi.org/10.1002/pssb.19660150224>
- Hanket, G. M., Boyle, J. H., Shafarman, W. N., & Teeter, G. (2010). Wide-bandgap (AgCu)(InGa)Se₂ absorber layers deposited by three stage co-evaporation. *IEEE Photovoltaic Specialists Conference, 00342(2010)*, 3425–3429. <https://doi.org/10.1109/PVSC.2010.5614576>
- Hosen, B., Bahar, A. N., & Ali, K. (2017). Data in Brief Modeling and performance analysis dataset of a CIGS solar cell with ZnS buffer layer. *Data in Brief*, 14, 246–250. <https://doi.org/10.1016/j.dib.2017.07.054>
- Jackson, P., Wuerz, R., Hariskos, D., Lotter, E., Witte, W., & Powalla, M. (2016). Effects of heavy alkali elements in Cu(In,Ga)Se₂ solar cells with efficiencies up to 22.6%. *Phys. Status Solidi RRL*, 10(8), 583–586. <https://doi.org/10.1002/pssr.201600199>
- Khoshsirat, N., Yunus, N., & Hamidon, M. (2015). Analysis of absorber and buffer layer band gap grading on CIGS thin film solar cell performance using SCAPS. *Pertanika Journal of Science and Technology*, 23(2), 241–250. <https://www.researchgate.net/publication/281720102>
- Lv, H., Wu, H., Wu, X., Zheng, J. Z., & Liu, Y. (2022). Fabricating WS₂/Mn_{0.5}Cd_{0.5}S/CuInS₂ hierarchical tandem p-n heterojunction for highly efficient hydrogen production. *Applied Surface Science*, 593(April), 153448. <https://doi.org/10.1016/j.apsusc.2022.153448>
- Nya, T., Kenfack, D., Maurel, G., Wilson, G., Touolac, T., & Jean, N. (2019). Journal of King Saud University – Science Highlighting some layers properties in performances optimization of CIGSe based solar cells : Case of Cu(In,Ga)Se – ZnS. *Journal of King Saud University - Science*, 31(4), 1404–1413. <https://doi.org/10.1016/j.jksus.2018.03.026>
- Onuma, Y., Takeuchi, K., Ichikawa, S., Harada, M., Tanaka, H., Koizumi, A., & Miyajima, Y. (2001). Preparation and characterization of CuInS₂ thin films solar cells with large grain. *Solar Energy Materials and Solar Cells*, 69(3), 261–269. [https://doi.org/10.1016/S0927-0248\(00\)00395-0](https://doi.org/10.1016/S0927-0248(00)00395-0)
- Phung, H., & Do, P. H. (2021). Scaps simulation of ZnO/In₂S₃/Cu₂Sn₃S₇/Mo solar cell scaps simulation of ZnO/In₂S₃/Cu₂Sn₃S₇/Mo solar cell. *Journal of Science and Technology*, 54(2016), 183–189. <https://doi.org/10.15625/2525-2518/54/1A/11824>
- Regmi, G., Ashok, A., Chawla, P., Semalti, P., Velumani, S., Sharma, S. N., & Castaneda, H. (2020). Perspectives of chalcopyrite-based CIGSe thin-film solar cell: a review. *Journal of Materials Science: Materials in Electronics*, 31(10), 7286–7314. <https://doi.org/10.1007/s10854-020-03338-2>
- Revathi, N., Prathap, P., Miles, R. W., & Reddy, K. T. R. (2010). Solar Energy Materials & Solar Cells Annealing effect on the physical properties of evaporated In₂S₃ films. *Solar Energy Materials and Solar Cells*, 94(9), 1487–1491. <https://doi.org/10.1016/j.solmat.2010.02.044>
- Revathi, N., Prathap, P., & Reddy, K. T. R. (2009). Thickness dependent physical properties of close space evaporated In₂S₃ films. *Solid State Sciences*, 11(7), 1288–1296. <https://doi.org/10.1016/j.solidstatesciences.2009.04.019>
- Salim, K. (2017). *Etude par simulation numérique d'une cellule solaire en CIGS Etude par simulation numérique d'une cellule solaire en CIGS*. Université Mohamed Khider Biskra.
- Santhosh, M. V., Deepu, D. R., Kartha, C. S., Kumar, K. R., & Vijayakumar, K. P. (2014). All sprayed ITO-free CuInS₂/In₂S₃ solar cells. *Solar Energy*, 108(2014), 508–514. <https://doi.org/10.1016/j.solener.2014.07.001>
- Shang, X., Wang, Z., Li, M., Zhang, L., Fang, J., Tai, J., & He, Y. (2014). A numerical simulation study of CuInS₂ solar cells. *Thin Solid Films*, 550, 649–653. <https://doi.org/10.1016/j.tsf.2013.10.047>
- Sharma, R. K., Chouryal, Y. N., Chaudhari, S., Saravanakumar, J., Dey, S. R., & Ghosh, P. (2017). Adsorption-Driven Catalytic and Photocatalytic Activity of Phase Tuned In₂S₃ Nanocrystals Synthesized via Ionic Liquids. *ACS Applied Materials and Interfaces*, 9(13), 11651–11661. <https://doi.org/10.1021/acsami.7b01092>
- Silvaco, I. (2019). *Atlas User's Manual, Device Simulation Software*. 408, 567–1000. <https://silvaco.com>
- Song, Z., Phillips, A. B., Xie, Y., Khanal, R. R., & Heben, M. J. (2013). The Performance of Nanocrystalline CuInS₂/In₂S₃/SnO₂ Heterojunction Solar Cells Prepared by Chemical Spray Pyrolysis. *IEEE*, 2540–2544. <https://doi.org/10.1109/PVSC.2013.6744992>
- Stutenbaeumer, U., & Mesfin, B. (1999). Equivalent model of monocrystalline, polycrystalline and amorphous silicon solar cells. *Renewable Energy*, 18(4), 501–512. [https://doi.org/10.1016/S0960-1481\(98\)00813-1](https://doi.org/10.1016/S0960-1481(98)00813-1)
- Sutanto, H., Durri, S., Wibowo, S., Hadiyanto, H., & Hidayanto, E. (2016). Rootlike Morphology of ZnO:Al Thin Film Deposited on Amorphous Glass Substrate by Sol-Gel Method. *Physics Research International*, 2016(3). <https://doi.org/10.1155/2016/4749587>
- Sutanto, H., Nurhasanah, I., Hidayanto, E., Wibowo, S., & Hadiyanto. (2015). Synthesis and characterization of ZnO:TiO₂ nano composites thin films deposited on glass substrate by sol-gel spray coating technique. *AIP Conference Proceedings*, 1699. <https://doi.org/10.1063/1.4938320>
- Sutanto, H., Wibowo, S., Hadiyanto, Arifin, M., & Hidayanto, E. (2017). Photocatalytic activity of cobalt-doped zinc oxide thin film prepared using the spray coating technique. *Materials Research Express*, 4(7). <https://doi.org/10.1088/2053-1591/aa7310>
- Sutanto, H., Wibowo, S., Nurhasanah, I., Hidayanto, E., & Hadiyanto, H. (2016). Ag doped ZnO thin films synthesized by spray coating technique for methylene blue photodegradation under UV irradiation. *International Journal of Chemical Engineering*, 2016(6195326), 1–6. <https://doi.org/10.1155/2016/6195326>
- Sylla, A., Ignace, N. A., Siaka, T., Vilcot, J., Sylla, A., Ignace, N. A., Siaka, T., & Theoretical, J. V. (2021). Theoretical analysis of the effect of the interfacial MoSe₂ layer in CIGS-based solar cells. *Open Journal of Modelling and Simulation*, 09(4), 339–350. <https://doi.org/10.4236/ojmsi.2021.94022>
- Taraque, M. A. R., Chowdhury, F. S., & Hasanat, L. Y. (2019). Design of Single Junction Si Solar Cell and Its Efficiency Investigation Using SILVACO ATLAS. *National Conference on Physics For Technology Development, December 2012*, 0–4. <https://www.researchgate.net/publication/332230309>
- Tchakpedeou, A.-B., Lare, Y., Napo, K., & Foussemi, A. (2022). An Improved Levenberg–Marquardt Approach With a New Reduced Form for the Identification of Parameters of the One-Diode Photovoltaic Model. *Journal of Solar Energy Engineering*, 144(4). <https://doi.org/10.1115/1.4053624>
- Theresa, T., Mathew, M., Kartha, C. S., Vijayakumar, K. P., Abe, T., & Kashiwaba, Y. (2005). CuInS₂/In₂S₃ thin film solar cell using spray pyrolysis technique having 9.5% efficiency. *Solar Energy Materials and Solar Cells*, 89(2005), 27–36. <https://doi.org/10.1016/j.solmat.2004.12.005>
- Thirumalaisamy, L., Palanivel, S., Raliya, R., Kavadiya, S., Sethuraman, K., & Biswas, P. (2019). Single-step growth of CuInS₂ nanospheres morphology thin films by electrospray chemical aerosol deposition technique. *Materials Letters*, 238, 206–209. <https://doi.org/10.1016/j.matlet.2018.12.021>
- Thomas, T., Kumar, K. R., Kartha, C. S., & Vijayakumar, K. P. (2015). Simple ‘one step’ spray process for CuInS₂/In₂S₃ heterojunctions on flexible substrates for photovoltaic applications. *Thin Films for Solar and Energy Technology VII*, 9561(95610J), 1–6. <https://doi.org/10.1117/12.2187065>
- Tobbeche, S., Kalache, S., Elbar, M., Kateb, M. N., & Serdouk, M. R. (2019). Improvement of the CIGS solar cell performance: structure based on a ZnS buffer layer Improvement of the CIGS solar cell performance: structure based on a ZnS buffer layer. *Optical and Quantum Electronics*, 51:284(August), 1–13. <https://doi.org/10.1007/s11082-019-2000-z>
- Trigo, J. F. A., Asenjo, B., Herrero, J., & Gutie, M. T. (2008). Solar Energy

- Materials & Solar Cells Optical characterization of In₂S₃ solar cell buffer layers grown by chemical bath and physical vapor deposition. *Solar Energy Materials & Solar Cells*, 92(2008), 1145–1148. <https://doi.org/10.1016/j.solmat.2008.04.002>
- Wai, H. S. (2022). Effect of Aluminum Doping Ratios on the Properties of Aluminum-Doped Zinc Oxide Films Deposited by Mist Chemical Vapor Deposition Method Applying for Photocatalysis. *Nanomaterials Article*, 12(195), 1–11. <https://doi.org/10.3390/nano12020195>
- Wang, A., & Xuan, Y. (2017). A detailed study on loss processes in solar cells. *Energy*. <https://doi.org/10.1016/j.energy.2017.12.058>
- Wijesundera, R. P., & Siripala, W. (2004). Preparation of CuInS₂ thin films by electrodeposition and sulphurisation for applications in solar cells. *Solar Energy Materials & Solar Cells*, 81(2004), 147–154. <https://doi.org/10.1016/j.solmat.2003.09.002>
- Wijewardane, S., & Kazmerski, L. L. (2023). Inventions, innovations, and new technologies: Flexible and lightweight thin-film solar PV based on CIGS, CdTe, and a-Si:H. *Solar Compass*, 7(May), 100053. <https://doi.org/10.1016/j.solcom.2023.100053>
- Yang, Q., Yang, S., Xi, T., Li, H., Yi, J., & Zhong, J. (2022). Gradient doping simulation of perovskite solar cells with CH₃NH₃Sn_{1-x}Pb_xI₃ as the absorber layer. *Current Applied Physics*, 44(August), 55–62. <https://doi.org/10.1016/j.cap.2022.08.012>



© 2023. The Author(s). This article is an open access article distributed under the terms and conditions of the Creative Commons Attribution-ShareAlike 4.0 (CC BY-SA) International License (<http://creativecommons.org/licenses/by-sa/4.0/>)